Pure Appl. Geophys. 172 (2015), 295–308

DOI 10.1007/s00024-014-0953-1

Pure and Applied Geophysics

A New Seismic Data Set on the Depth of the Moho in the Alps

Irene Bianchi,[1] Michael Behm,[1,2] Eva Maria Rumpfhuber,[3] and Götz Bokelmann[1]

Abstract—We present the results from receiver function analysis applied to a comprehensive data set in the Eastern Alps. Teleseismic events were recorded at 70 stations with an average deployment of 1 year. The investigated area includes the eastern part of the Eastern Alps and their transition to the Bohemian Massif, the Pannonian domain, and the Southern Alps. The crustal structure at each station is examined with the Zhu-Kanamori (ZK) method, which yields well-resolved interface depths in laterally homogeneous media with limited layering. The application of the ZK technique is challenged because of the complex tectonic setting; therefore, we include additional constraints from recent active-source seismic studies. In particular, the well-known crustal P-wave velocity and, where available, the V_p/V_s ratio are kept fixed, thus reducing the ambiguity in determining Moho depths. Individual depth values vary strongly between adjacent stations, showing that the employment of the ZK technique in tectonically complex settings is limited. We therefore avoid interpreting the results in detail, but rather compare them to existing crustal models of the Eastern Alps. We regard this receiver function study in the easternmost part of the Alps as a documentation of a data set that has potential to be exploited in the future.

Key words: Eastern Alps, Moho, receiver functions, crustal structure, ZK technique.

1. Introduction

The Alps formed during the convergence between the European and African plates. Besides these two major plates, a number of smaller tectonic fragments were involved in the construction of the present-day Alpine architecture. Paleogeographic reconstructions describe the progressive consumption of the Meliata and then of the Piemont-Ligurian Ocean by Late Cretaceous; continental collision started in the Middle Eocene, involving several hundreds of kilometers of shortening causing the formation of thick lithospheric roots (e.g., Panza *et al*. 1980; Babuska *et al*. 1987). The Eastern Alps (EA) were later affected by the roll back of the Carpathian subduction (Royden *et al*. 1983) in the Late Oligocene-Early Miocene, and reacted with the onset of an escape tectonic regime (Ratschbacher *et al*. 1991) as indicated by dextral transpression in the south (Periadriatic line) and sinistral, strike-slip dominated kinematics in the north (e.g., SEMP line, Mur-Muerz-line). Based on recent seismic investigations and a wealth of complimentary geodynamic observations, Brückl *et al*. (2010) and Brückl (2011) provide a kinematic model for post-collision and escape tectonics. The authors postulate a stable continental triple junction in between the European plate, Adriatic foreland, and Pannonian fragment. In the context of this complex geodynamic setting, the Moho is expected to have been considerably modified since the onset of convergence. Subduction consumed many hundreds of kilometers of crust and mantle lithosphere (e.g., Dewey *et al*. 1973; Laubscher 1990; Ustaszewski *et al*. 2008), and a newly formed Moho has potentially been developed in the subducted continental crust by high-pressure metamorphism (Laubscher 1990). Crustal thinning during escape/extension further modified the Moho topography (Ratschbacher *et al*. 1991), in particular at the plate boundaries.

Information on crustal thickness in the Eastern Alps is derived mainly from vintage to recent active source 2D and 3D experiments (Alpine Explosion Seismology Group 1976; Yan and Mechie 1989; Guterch *et al*. 2003; Brückl *et al*. 2003, 2007; Lueschen *et al*. 2004; Bleibinhaus and Gebrande 2006; Behm *et al*. 2007; Grad *et al*. 2009a; Behm

Electronic supplementary material The online version of this article (doi:10.1007/s00024-014-0953-1) contains supplementary material, which is available to authorized users.

[1] Department of Meteorology and Geophysics, University of Vienna, Vienna, Austria. E-mail: irene.bianchi@univie.ac.at
[2] Department of Geophysics, Colorado School of Mines, Golden, CO, USA.
[3] ExxonMobil Exploration Company, Houston, TX, USA.

2009). Teleseismic studies in the Western and Eastern Alps (Lippitsch *et al*. 2003; Dando *et al*. 2011; Mitterbauer *et al*. 2011) targeted the deep lithosphere and contribute to an ongoing debate on slab geometry and subsequent geodynamic implications (e.g., Kissling *et al*. 2006; Brückl 2011).

Geissler *et al*. (2008) produced a Moho map for central and Eastern Europe using receiver functions, which gives coarse information on the crustal structure involving stations with a spacing of hundreds kilometers. Gravimetric measurements (Meurers and Reuss 2009) help determine the crustal thickness, even though their sensitivity to shallow crust or mantle anomalies makes the results non-unique. Grad *et al*. (2009b) present a Moho map of the entire European plate based on 2D and 3D active source seismic data, surface wave and receiver function studies, as well as gravity models. Di Stefano *et al*. (2011) and Spada *et al*. (2013) provide maps for the Alpine area based on integrating passive and active seismology.

As stated above, many different techniques can provide information on crustal structures. One of them, the receiver function (RF) method, is based on converted teleseismic body waves and has become a popular and successful method, in particular for obtaining estimates of crustal thickness (e.g., Zhu and Kanamori 2000; Dugda *et al*. 2005). RF studies in the western part of the Alps (Lombardi *et al*. 2008, 2009) have aimed at unraveling the Moho and deeper discontinuities. In the Eastern Alps, the first and to date only published RF analysis on a crustal scale was applied along the TRANSALP profile (Kummerow *et al*. 2004). Our study presents a new comprehensive RF data set covering a large portion of the Eastern Alps and inferred insights into crustal structure and thickness.

The information about the Moho from the different seismic techniques is dependent on the resolution capabilities of each methodology. To a large extent, the resolution and imaging depth depend on the frequency content of the employed seismic source (e.g., low-energy, high-frequency CSS data vs. high-energy, low-frequency earthquake data). It is important to recognize that the knowledge obtained about the crust-mantle transition strongly depends on the applied techniques and their intrinsic resolution capabilities (Carbonell *et al*. 2013). Given the existing wealth of CSS data in the Eastern Alps, we aim to add complementary information on crustal structures, in particular the Moho topography, from earthquake data.

We apply the method developed by Zhu and Kanamori (2000) (ZK) to the data and exploit the 20-km narrow spacing of 70 temporary and permanent seismic stations. The ZK technique has been applied worldwide in multiple studies (e.g., França and Assumpçao 2004; Geissler *et al*. 2008; Piana Agostinetti and Amato 2009; Lloyd *et al*. 2010; Gallacher and Bastow 2012) and is a well-established method to estimate depths and V_p/V_s ratios for simple crustal structures. Complex tectonic environments prove to be a challenge for ZK technique, since the RF time series are composed of a multitude of converted phases due to the occurrence of several seismic discontinuities in the crust (e.g., Champion *et al*. 2006). Due to the intricate structure of the Eastern Alps, we chose to constrain the results by keeping the V_p/V_s ratio constant and invert for Moho depths only. We further validate our results with previously published Moho depths.

2. *Data and Method*

2.1. *Receiver Function Data set*

We use data collected from three seismic networks for a total of 70 locations. Forty-nine stations belong to the ALPASS temporary network (Mitterbauer *et al*. 2011), 15 to the CBP (Carpathian Basin Project) temporary network (Dando *et al*. 2011), and 6 to the Austrian seismological permanent network (maintained by ZAMG, Zentralanstalt für Meteorologie und Geodynamik, http://www.zamg.ac.at). The stations are located between 11°E and 17°E longitude and between 45.5°N and 49°N latitude (Fig. 1). The ALPASS stations recorded between July 2005 and April 2006, and CBP stations were active from May 2006 to June 2007. In addition, data recorded between January 2009 and June 2011 by the ZAMG network are included in this study.

We calculate RFs from earthquakes that occurred at epicentral distances ranging from 25° to 110° and

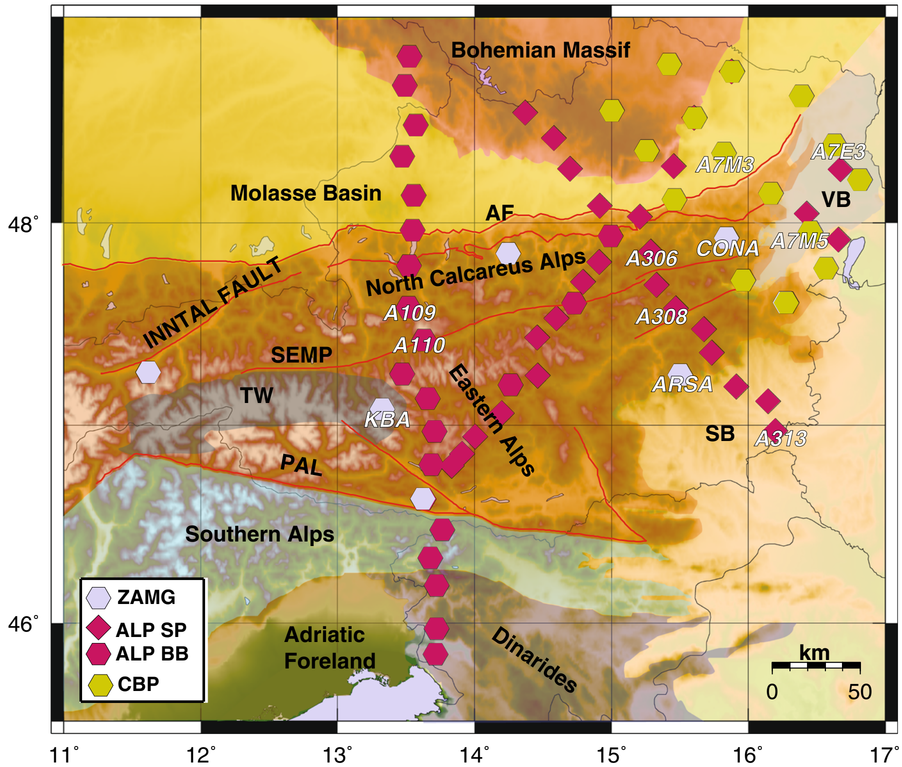

Figure 1
Map of the Eastern Alps with station location. *Red lines* draw the path of major tectonic lines (*AF* Alpine thrust front, *PAL* Periadriatic Line). Names for the different tectonic domains are written on *shaded areas* (*TW* Tauern Window, *VB* Vienna Basin, *SB* Styria Basin). *Hexagons* represent the Broad Band station locations; *diamonds* are short period stations; *colors* are related to different networks

with a magnitude $M_b > 5.5$. Figure 2a illustrates the epicenters of teleseismic events recorded by the permanent network between January 2009 and June 2011 (gray stars). The earthquakes used for the RF computation are shown as blue stars for station ARSA and yellow stars for station MOA. These two stations include the largest and smallest selected data set. Histograms of the back azimuth angle and epicentral distances are shown in Fig. 2b and c. All epicentral distances are sufficiently covered with a maximum at 80°–90°; the bulk of discarded events (gray bars in Fig. 2c) is associated with epicentral distances larger than 95°. The south and southwest directions are less sampled with respect to back azimuthal angles (Fig. 2b).

P-S receiver functions highlight the differential arrival time between the P-wave and the P-to-S converted wave (Ps) at a major seismic interface (Langston 1979; Ammon 1991). The arrival time of the Ps phase relative to the arrival time of the P phase is a proxy of the depth of the converting interface. The presence of several interfaces causes various Ps converted phases along with their multiples (PpPs, PsPs + PpSs phases). Therefore, a complicated crustal structure results in a more complex RF with more than one phase. The RFs are computed on two planes, the radial (plane joining the source with the station, positive from the source) and the transverse (at 90° clockwise from the radial plane). For an isotropic medium, the converted Ps phases are present only on the radial component, since the S converted wave is polarized on the radial plane only. For anisotropic structures, however, the converted S-waves are polarized according to the fast and slow anisotropic planes; therefore, the signature of the Ps conversions appears on both the radial and transverse components. This study considers only the radial component of the RF in order to obtain the average crustal thickness below each seismic station. The receiver functions are calculated by a frequency

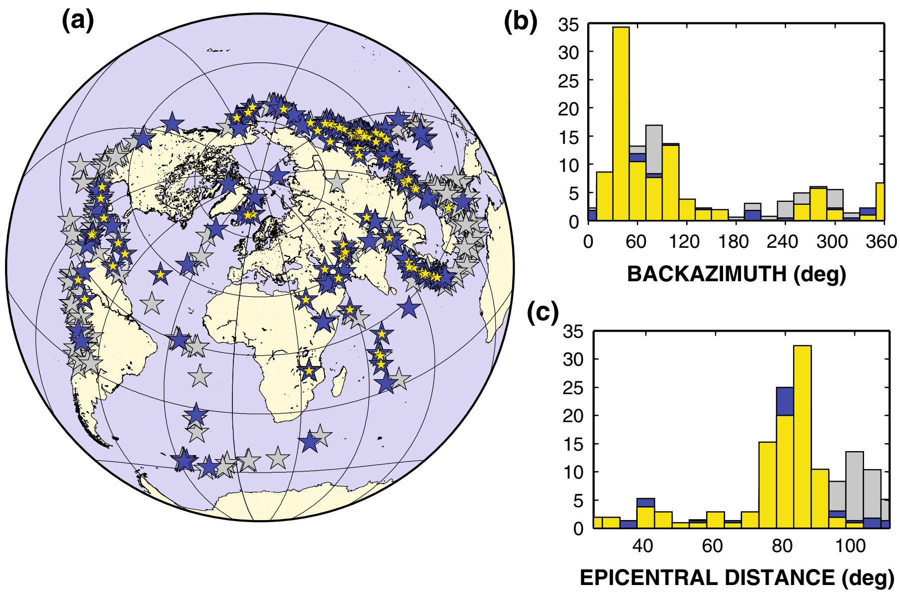

Figure 2

a Epicentral distribution of teleseismic events. *Gray stars* show events between 2009 and 2011, *blue stars* events recorded by station ARSA, and *yellow stars* events recorded by station MOA. **b** Back azimuthal distribution of the teleseismic events displayed on the map with same color coding as for (**a**). **c** Epicentral distance distribution of the events displayed on the map with same color coding as for (**a**)

domain algorithm using multitaper correlation estimates (Park and Levin 2000). The method provides an estimate of RF uncertainty in the frequency domain, using the pre-event noise spectrum for frequency-dependent damping. The multitaper spectrum estimates are leakage resistant, so low-amplitude portions of the P-wave spectrum can contribute to the RF estimate. This enables RFs from different seismic events to be combined in a weighted-average RF estimate. In our study, the weighted average RFs are obtained by binning events at 10° wide intervals of epicentral distance from all back azimuthal directions. By stacking receiver functions from different directions (azimuths), effects of lateral structure variation are suppressed, and an average crustal model is obtained.

A high pass filter with a cutoff frequency at 1 Hz is applied, which results in a vertical RF resolution of approximately 2–3 km.

The RF sets for each station are grouped in six quality classes (1—best data to 5—poor data; 6 for discarded data). The classification has been performed according to the following observations on the RF sets: (1) identification of the Ps-Moho phase, (2) total back azimuthal coverage, (3) presence of clear multiples, (4) absence of reverberations from sedimentary shallow layers, and (5) absence of strong intracrustal or upper mantle converted phases. According to these observations, the RF gathers are grouped in quality classes 1–6. RF sets for which all constraints are observed are grouped in quality class 1 (i.e., ARSA). When there is no clear identification of the Ps-Moho phase and none of the constraints are fulfilled, the station is discarded (e.g., A106). Examples for each class are shown as supplementary online material.

A minimum number of 28 and a maximum number of 229 RFs have been used at individual stations. In Fig. 3, RF gathers are grouped based on similar features, in particular phases, amplitudes, and arrival times, and on both station location and recording length of the station. ARSA and CONA have data classified in quality one and two, respectively. For station ARSA (Fig. 3a), the Moho pulse is well identified together with the multiples; an earlier pulse (labeled Psc) is identified, likely because of an intracrustal interface. RFs at CONA (Fig. 3b) show the Moho converted phase (Psm) together with its multiples and the Psc phase; in this example, the Psc phase has a larger amplitude than the Psm. The

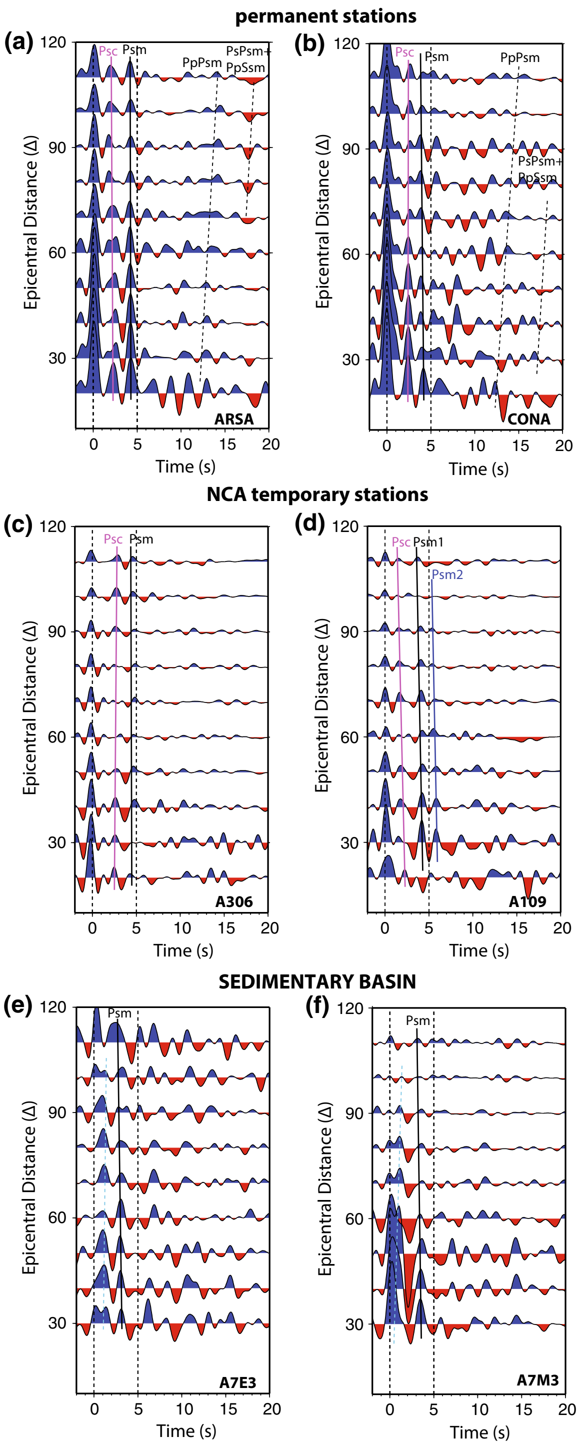

Figure 3

Data examples. Radial RFs are computed using a frequency cutoff of 1 Hz and binned according to their epicentral distance (10° bins). Moho (Psm) converted phase and intracrustal (Psc) phase are indicated along the epicentral sweep with their multiples when visible. **a**, **b** Stations belonging to the permanent network and located in the Eastern Alps s.s. and North Calcareous Alps (NCA). **c**, **d** Stations located in the NCA and belonging to the temporary network. **d** Converted phases at larger depths are highlighted as Psm1 and Psm2. **e**, **f** Stations located on the sedimentary basin, Vienna Basin, and Molasse Basin, respectively

arrival time of the Psc (2.5 s) would correspond to an interface at a depth of less than 20 km, which is incompatible with the average Moho depth (~35 km) in the area from previous studies (i.e., Grad *et al.* 2009b; Behm *et al.* 2007). The Psc conversion might be due to a strong intracrustal discontinuity and/or a velocity gradient in the lower crust. The occurrence of this high amplitude Psc phase downgrades the quality of the observation at CONA from class 1 to class 2. The arrival times of the multiple phases can clearly be identified at stations of the permanent network (Fig. 3a, b), because of its large number of recorded events and the station's high-quality installation. Stations A306 and A109 are classified in quality 3. Both of them show Psc and Psm phases, and A109 has a third important phase identified as Psm2. These two stations hold the kind of information that we get from some temporary stations in the study area, with the presence of two or three converted phases at depth. The two stations in Fig. 3e and f are located within the Vienna Basin and Molasse Basin, respectively, and they have been classified in quality class 3. The first seconds of the RF waveform for these two stations are occupied by the reverberations due to the sedimentary cover (pulses highlighted by the blue dashed line); however, the Moho converted phase (indicated as Psm) is still visible.

2.2. *Application of the ZK Method*

The crust-mantle boundary (Moho) is the most pronounced seismic contrast in the lithosphere; therefore, the Ps phases converted at the Moho (Psm) dominate the RF time series. In an RF waveform, the time difference between the direct P-wave and the P-to-s converted phase at the Moho is used to estimate the crustal thickness. However, the time difference is dependent on both the compressional wave velocity (V_p) of the crust and its V_p/V_s

ratio. The ZK technique uses the relationship between the differential arrival time of the RF, the thickness, and the velocities within this layer. The method employs a grid search in the two-dimensional domain defined by the layer thickness (H) and V_p/V_s ratio (k) for a set of specified average V_p velocities (e.g., 6.0, 6.5, 7.0 km/s). A stacking function S (H,k) is defined as $S\ (H,\ k) = w_1 r(t_1) + w_2 r(t_2) - w_3 r(t_3)$, where $r(t)$ is the amplitude of the radial RF; t_1, t_2, and t_3 are the predicted Ps, PpPs, and PpSs + PsPs arrival time corresponding to H and k; and $w_{1,2,3}$ are the phase weights. We chose the weights for the converted and reflected phases (w_1, w_2 and w_3 for Ps, PpPs, and PpSs + PsPs), as 0.7, 0.2, and 0.1, respectively, based on Zhu and Kanamori (2000). The sum S (H, k) is performed for all the RF from the different epicentral distances. For simple crustal structures, the technique yields a well-resolved maximum and unique result for the Moho depth in the grid search. However, in the presence of a layered crust, multiple pronounced local maxima are observed (e.g., Eaton *et al.* 2006; Olsson *et al.* 2008).

A grid search for both H and k shows multiple maxima among which the H and k values maximizing the S-function reach unrealistically high and low values at many stations. Examples of the S (H, k) function are shown in the supplementary online material (Figure S1).

We aim to minimize the non-uniqueness of possible (H, k) solutions by calculating the stacking function for fixed V_p and V_p/V_s ratios at each station. The stacking function is referred to as S (H), since it only depends on the crustal thickness H. The V_p and V_p/V_s values at each station are based on the crustal models of Behm *et al.* (2007) and Behm (2009). In these studies, the average crustal V_p varies between 6 km/s, e.g., in the Molasse Basin region, and 6.6 km/s in the southern part of the Bohemian Massif. V_s has only been constrained in the upper crust at a number of stations, and the observed V_p/V_s ratios range between 1.73 and 1.83. At a global scale, a higher V_p/V_s ratio in the crust is caused by above-average V_p (e.g., mafic rocks) rather than by an anomalously low V_s. Previous studies do not indicate increased V_p velocities in the middle and lower crust in our study area, with the exception of the southern

Table 1

Station names and coordinates

Station	Lon	Lat	z_1 (km)	z_2(km)	z_3 (km)	Moho (km)	σ (km)	Q
A102	13.54	48.81	24	38	60	38	4	4
A103	13.51	48.67	*	37	*	37	3	4
A104	13.59	48.48	24	35	*	35	4	5
A105	13.49	48.33	*	29	*	29	2	5
A106	13.57	48.14	*	*	*	*	–	6
A107	13.57	47.96	22	44	*	44	3	5
A108	13.54	47.79	25	41	*	41	3	5
A109	13.54	47.59	21	35	48	48	5	3
A110	13.65	47.42	22	30	45	45	4	5
A111	13.49	47.26	*	45	68	45	3	5
A112	13.68	47.13	21	40	66	40	4	5
A113	13.73	46.97	23	40	*	40	3	4
A114	13.7	46.8	22	41	66	41	3	4
A115	13.65	46.63	22	*	*	*	–	6
A116	13.78	46.47	20	42	*	42	2	3
A117	13.69	46.33	*	37	*	37	3	4
A118	13.74	46.19	24	43	62	43	3	3
A119	13.74	45.97	22	44	69	44	3	3
A120	13.73	45.84	*	44	*	44	5	3
A202	15.9	48.74	22	30	*	30	3	2
A204	15.62	48.51	20	28	45	28	5	5
A206	15.48	48.28	22	39	*	39	4	3
A208	15.22	48.03	28	40	*	40	6	3
A210	14.93	47.81	25	41	*	41	3	4
A211	14.81	47.71	28	47	*	47	6	4
A212	14.74	47.61	*	36	63	36	6	3
A213	14.62	47.53	24	43	*	43	9	5
A214	14.48	47.44	32	45	62	45	3	5
A215	14.48	47.25	21	38	65	38	3	3
A216	14.28	47.2	*	39	60	39	4	2
A217	14.22	47.06	*	*	*	*	–	6
A218	14.02	46.94	24	38	62	38	4	4
A219	13.93	46.86	24	43	57	43	3	4
A220	13.85	46.8	*	34	50	34	4	3
A301	14.39	48.54	*	*	*	*	–	6
A302	14.6	48.42	22	36	64	36	5	5
A303	14.71	48.27	*	40	56	40	4	4
A304	14.93	48.08	*	42	*	42	2	4
A305	15.01	47.94	21	32	*	32	3	5
A306	15.3	47.86	23	38	*	38	3	3
A307	15.35	47.7	*	47	62	47	3	4
A308	15.49	47.58	22	30	42	42	2	5
A309	15.69	47.48	24	36	51	36	2	5
A310	15.75	47.36	21	33	*	33	3	4
A311	15.93	47.19	21	37	53	37	5	5
A312	16.16	47.12	22	35	*	35	3	4
A313	16.22	46.97	*	32	61	32	6	5
A401	16.68	47.92	24	37	*	37	3	5
A402	16.69	48.26	22	36	52	36	6	4
A403	16.45	48.05	*	29	47	29	3	4
A404	16.29	47.61	22	32	*	32	3	3
A7E1	15.9	48.74	21	30	42	30	4	2

Asterisk indicates absence of the interface

z_1, z_2, and z_3 correspond to the interface depth identified at each station. Moho depth and σ in km and the quality class (Q) are reported part of the Bohemian Massif and the wider Vienna Basin region. For the Bohemian Massif, V_s velocities are obtained for the entire crustal column and do not result in an increased V_p/V_s ratio. The V_s model does not cover the Vienna Basin region where both seismic and gravimetric data (Tierno Ros 2009) suggest anomalously high values for V_p and densities, indicating an extensive presence of mafic rocks. Taking the thick sedimentary layer of the Vienna Basin further into account, we assume a V_p/V_s ratio of 1.83 for stations located within the basin and its surroundings. With regard to the V_p/V_s ratio of the upper crust and due to the absence of anomalous high V_p in the middle and lower crust outside the previously mentioned regions, we chose a V_p/V_s ratio of 1.73 for all other stations. The search for H is constrained between 20 and 70 km depth.

2.3. Identification of Interfaces

The application of the ZK technique to the data set results in 70 S (H) functions. Many of them feature more than one maximum, possibly also because of the presence of layering within the crust. The maxima of the S (H) functions were extracted and are listed in Table 1. Each station displays between one and three local maxima [examples of the S (H) function are shown in Fig. 4]. The shallowest maximum is located between 20 and 25 km, the intermediate between 28 and 47 km depth, and the deepest between 42 and 68 km; these are named respectively z_1, z_2, and z_3 in Table 1. We refer the

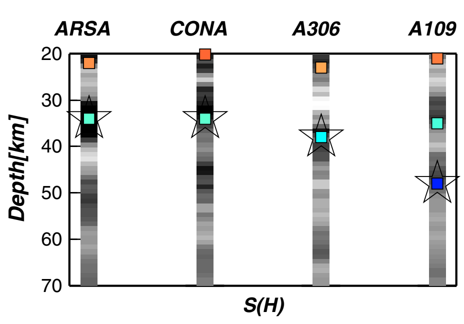

Figure 4
Example of S (H) for stations displaying more than one maximum for the stations in Fig. 3. *Darker colors* for higher values of S (H) and lighter for lower values. *Colored squares* (*color scale* as in Fig. 6) highlight maxima. *Stars* mark the maximum associated with the Moho depth

first (z_1) to a mid-crustal interface, the second (z_2) to the Moho, and the third (z_3) to a converter located in the uppermost mantle. Exceptions are encountered for stations A109, A110, A308, and KBA, for which we refer to the deeper interface (z_3) than the Moho. The deeper interface at stations A109 and A110 keeps continuity with the neighboring stations. At station A308, the depth of the third interface (z_3) is in agreement with the Moho depth for the northward neighboring station, while the depth of the second interface (z_2) agrees with the Moho depth detected for the southward neighboring station, rendering the location of A308 a possible site witnessing two Mohos overlap. At station KBA, the third interface (z_3) shows a slightly deeper Moho (at 54 km depth) with respect to previous studies on the same site [49 km in Behm *et al.* (2007)].

We approximate the selected maximum of the S (H) function at each station with a Gaussian function in order to constrain the uncertainty on the Moho depth. The variance of the Gaussian function defines the depth uncertainty as shown in Figure S2. A broader S (H) function is due to broader Ps pulses or to the lack of multiples, and the resulting larger uncertainty might indicate a dipping Moho. Considering all RF sets, the uncertainties on Moho depths range from 2 to 9 km and are listed in Table 1. The average difference to Moho depths based on active source data amounts to −1.5 km, and the associated standard deviation is ±4.7 km. The low average difference indicates a good overall agreement with existing models. However, the considerably large standard deviation suggests that individual depth values must be interpreted with caution and that analyses of the result should only focus on the large-scale trends. Maxima above the Moho conversion are interpreted to be intracrustal interfaces, and deeper conversions result from interfaces in the uppermost mantle.

2.4. Synthetic Test

As outlined in the previous sections, the presence of multiple crustal interfaces is expected to limit the determination of accurate depths. In order to estimate the reliability of the ZK method, we perform a synthetic test, which includes a mid-crustal interface,

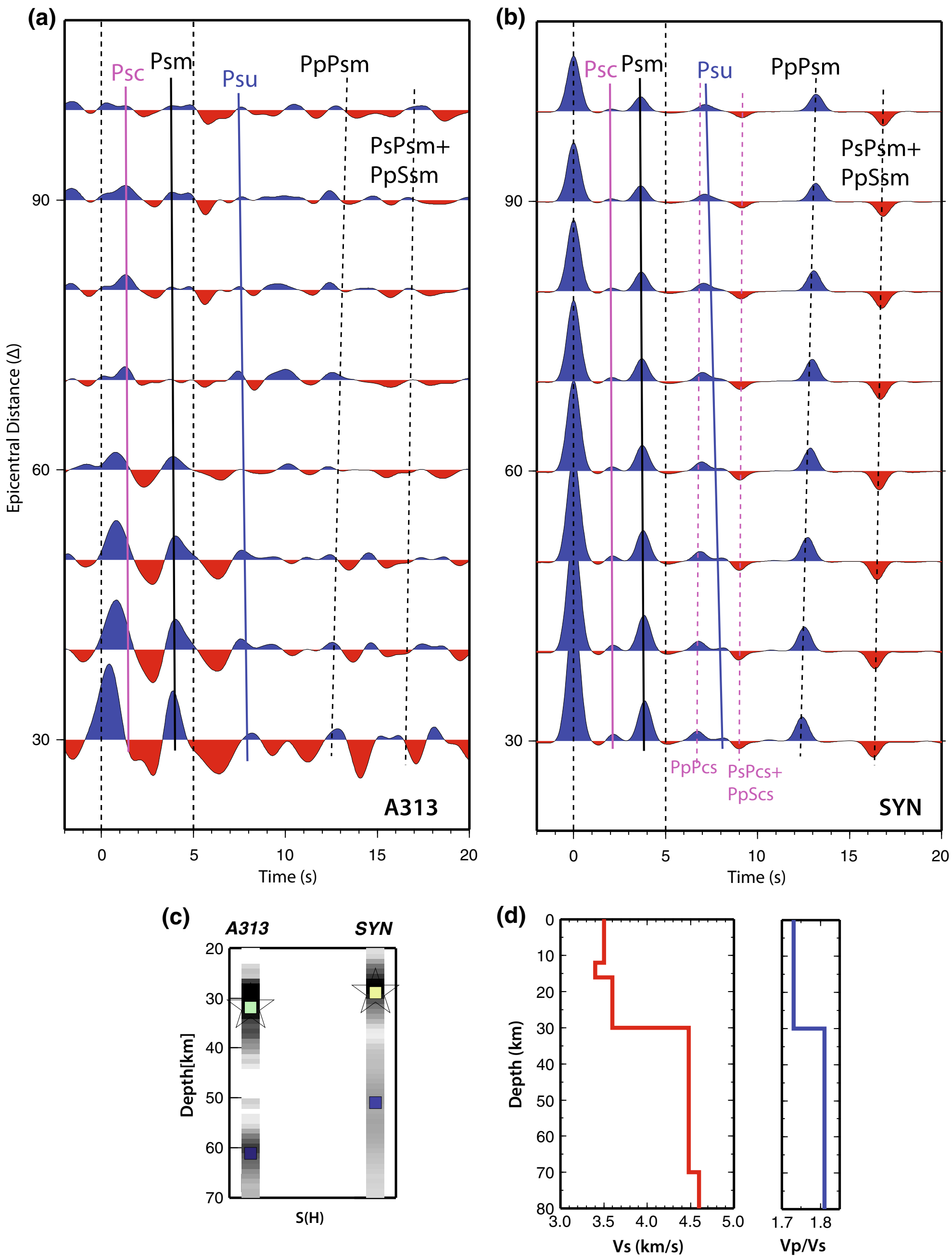

Figure 5

a RF from station A313. **b** Synthetics constructed from the model extracted from Yan and Mechie (1989). The 2D ALP75 section at coordinate N47.1°E16.2° would pass close to station A313. **c** *S* (*H*) for station A313 and SYN; maxima of the function *S* (*H*) are highlighted by *colored squares* (*color scale* as in Fig. 6); *stars* mark the Moho depth. **d** V_s and V_p/V_s at depth used for calculating the synthetic RFs

the Moho, and a reflector in the uppermost mantle (Fig. 5). The model is based on the refraction profile ALP75 that runs along the crest of the entire Alpine arc. We extract layer thickness and V_p velocities of the 2D ALP75 model (Yan and Mechie 1989), where the profile is close to station A313. The model features an intracrustal interface (velocity increase) at 16 km depth, a crustal thickness of 30 km, and an interface in the upper mantle at 70 km depth. The synthetic RF data set (Fig. 5b) is created using

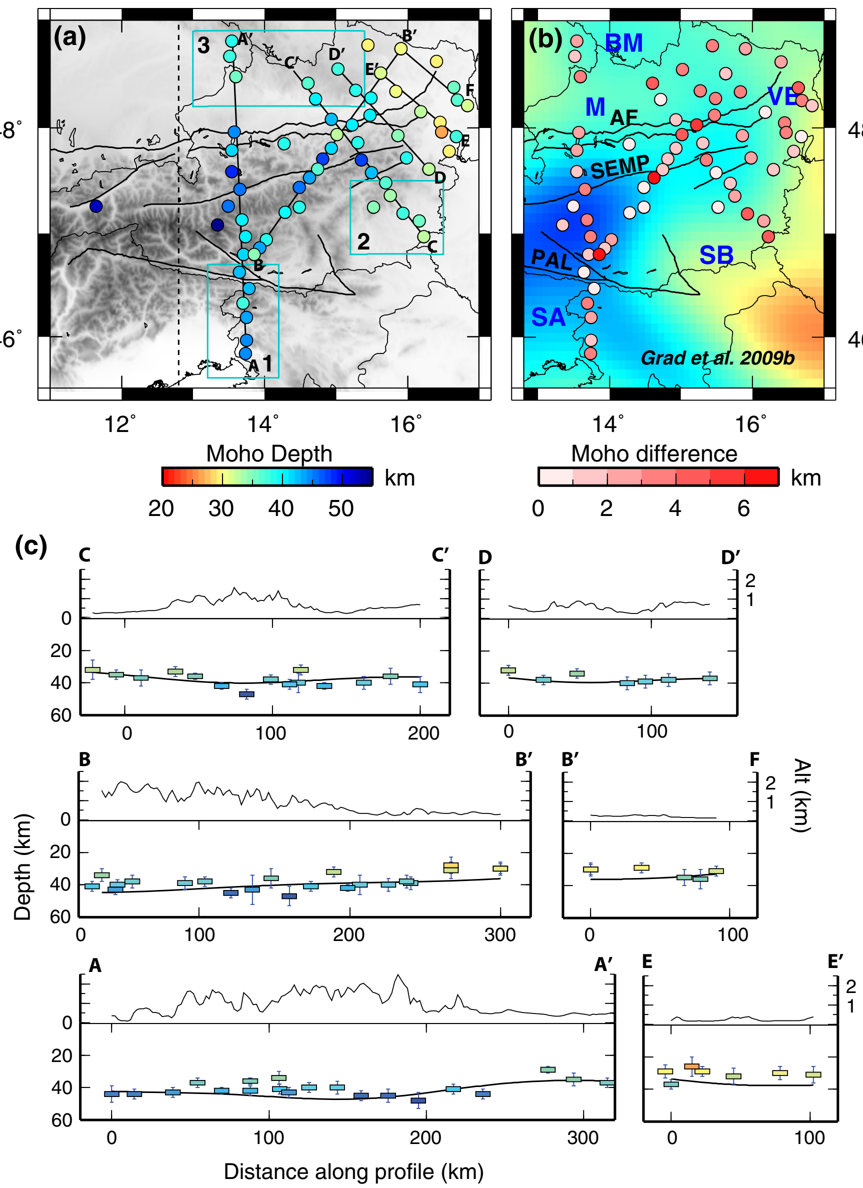

Figure 6

a Moho depths obtained by RF analysis (*circles*), topography in the background, *black solid lines* for major fault lines; *dashed line* isolates the area displayed in (**b**). **b** Moho map from Grad *et al*. (2009b) as background; *circles* show the depth difference between Moho depths retrieved in this study and depth from Grad *et al*. (2009b) at the station location. **c** *Colored rectangles* show Moho depths retrieved in this study along depth profiles whose traces are shown in Fig. 6a; the associated *blue bars* display uncertainty of Moho depth. The *black line* on profiles displays the Moho depth from Grad *et al*. (2009b)

RAYSUM (Frederiksen and Bostock 2000) and is compared to the observed receiver functions for station A313 (Fig. 5a). The Ps converted phases generated at each interface are marked Psc (intracrustal discontinuity), Psm (Moho), and Psu (upper mantle discontinuity). Multiples for Psc and Psm are clearly visible on the synthetic data set. The first multiple of the Psc overlaps in arrival times with Psu for large epicentral distances (80°–100°). The theoretical arrival times for Psm multiples are marked on the observed data set as well. We performed the search for the Moho depth on the synthetic data setting $V_p = 6.16$ km/s and $V_p/V_s = 1.73$, as we did for station A313. S (H) is displayed in Fig. 5c for the observed and the synthetic data set. In the synthetic case, the maximum S (H) value is reached for $H = 29$ km compared to the initial model of 30 km. In the observed case, the maximum in $S(H)$ is at $H = 32$ km. The depth to the intracrustal discontinuity is out of the minimum boundary of the search and cannot be detected in the synthetic case. The upper mantle discontinuity can be recognized (blue squares in Fig. 5c). The technique fails to determine the depth of the upper mantle reflector, since the mantle velocity and V_p/V_s have not been established. The local maximum is not as pronounced, and the inferred depth is 18 km too shallow. The constructed synthetic data set would be classified in quality class 1, as it fulfills all the observations described in Sect. 2.1, whereas A313 is in quality class 5. Station A313 has been chosen for its vicinity to the ALP75 profile, which describes the shallow (up to 70 km depth) structures of the lithosphere with a simple layered velocity model. We used this layered velocity model to test our method and retrieve the Moho depth. This simple synthetic test indicates that in the presence of an additional crustal interface, and with good knowledge of crustal velocities, Moho depths can be extracted accurately. However, it must be noted that more complex structures, in particular sedimentary basins, can significantly degrade the quality of RFs (e.g., Gans 2011).

3. Results and Discussion

In this section, we present and discuss the results of the RF analysis in terms of both Moho depth estimates and presence/absence of first-order intracrustal seismic discontinuities beneath the seismic stations. Our estimates of the depth of the crust-mantle boundary are compared to a recently published Moho map beneath the study area. The presence of intracrustal seismic discontinuities is discussed in light of the results from previously acquired seismic lines, which highlighted the occurrence of high-reflectivity layers across the Eastern Alpine region. Moho depth results are reported in Table 1, together with the depth of the intracrustal interface where constrained by the data. In Fig. 6, we show both the punctual estimates of Moho depth for each analyzed station (Fig. 6a), which can be readily compared to a previously published interpolated map, i.e., Grad *et al*. (2009b) (Fig. 6b). Superimposed on the Grad *et al*. (2009b) map, we show the difference between the latter and the Moho depths (considering depth uncertainty) obtained in this study (Fig. 6b).

3.1. Moho Depth

Moho depths retrieved at single stations are summarized in Table 1 and shown on the map in Fig. 6a. Our results for Moho depth are in good agreement with previous studies in areas less affected by Alpine tectonics. The three boxes in Fig. 6a display such areas: the Southern Alps (Box 1), Styria Basin (Box 2), and Molasse Basin and Bohemian Massif (Box 3). We extract the punctual estimate of Moho depth from Grad *et al*. (2009b) under each station in the area and directly compare this value to our estimate (considering depth uncertainty). In the Southern Alps, the Moho depth from our analysis is on average 42 ± 2 km; 39 km depth was found by Geissler *et al*. (2008) and ~40 km by Molinari *et al*. (2012); the differences between our results and extracted punctual depths from Grad *et al*. (2009b) are within 0 and 4 km. The retrieved Moho depth is 37 ± 1 km beneath the western part of the Molasse Basin and the Bohemian Massif, and extracted punctual depths from Grad *et al*. (2009b), beneath the station locations, differ from our results by 1–4 km. Moho below the Styria Basin is 34 ± 2 km deep, 31 km was found in Geissler *et al*. (2008), and the differences with extracted punctual depths at the station locations from Grad *et al*. (2009b) are within 1 and 4 km.

Maximum Moho depth in the area is found across the Tauern Window, reaching values as deep as 52–54 km. These values are comparable to previous results of the TRANSALP experiment (e.g., ~50 km in Castellarin *et al*. 2006; 48 km in Geissler *et al*. 2008). However, our results display a larger degree of variability for nearby stations, suggesting the presence of a complex structure in the lower crust within this portion of the orogens (see below).

Moho depths from RF provide additional information for the Vienna Basin region (30–34 km), which is not well constrained by active source data

(Behm *et al*. 2007). Below the Vienna Basin, a crustal thickness of less than 30 km was already shown in Molinari *et al*. (2012).

Depth differences with respect to Grad *et al*. (2009b) and pronounced scatter of individual RF Moho depths among adjacent stations are observed in the central area of the mountain chain, and this is bounded by the occurrence at the surface of the major faults (i.e., PAL and AF). The differences in Moho depth with respect to Grad *et al*. (2009b) reach 7 km and indicate a high degree of variability in our results (Fig. 6c). This difference compared to the reference study and scatter between adjacent stations could be related to the presence of anisotropy or furthermore a laminated lowermost crust. Examples of anisotropy in the lower crust have been published in recent years (e.g., Bischoff *et al*. 2006; Endrun *et al*. 2011; Roux *et al*. 2011); some studies state that anisotropy affects RF (e.g., Eckhardt and Rabbel 2011; Porter *et al*. 2011; Bianchi *et al*. 2010), and forward modeling of RF cannot match the data if anisotropy is not considered (e.g., Bianchi *et al*. 2008; Nagaya *et al*. 2008; Liu and Niu 2012). A number of geophysical processes affect the possibility of retrieving the Moho depth beneath an orogen. For example, eclogitization of the lower crust can alter the seismic properties directly above the Moho, biasing the recognition of crustal thickness (Wittlinger *et al*. 2009). Also, the occurrence of a Moho doubling, developed during the continental collision, can make recognizing the exact depth of the Moho very difficult (e.g., Piana Agostinetti *et al*. 2011). In the following, we briefly discuss some hypotheses about the scattering of the results.

We highlighted that, in some regions, individual Moho depths retrieved in this study scatter considerably among adjacent stations; moreover, they do not agree well in a point-by-point comparison with previously published models (i.e., Brückl *et al*. 2007; Behm *et al*. 2007; Grad *et al*. 2009b) even though the V_p and V_p/V_s values used for the computation of the S (H) stacking function have been extracted from these and related studies. The poor correlation between the Moho depths from RFs and wide-angle models is explained by one or more of the following factors: (1) The ZK technique encounters issues in complex tectonic environments and in case of a low S/N ratio. It is possible that some of the extracted maxima are a result of noise in the data set, lower crustal conversions, or multiple phases and therefore represent spurious energy instead of genuine Ps conversions. (2) RF and the wide-angle experiments sample the crustal structures with an order of magnitude of different wavelengths. (3) RFs are most sensitive to S-wave structure, while wide-angle experiments are sensitive only to P-wave structure. (4) Because of the large angles of incidence in wide-angle experiments, the travel times are sensitive to both the vertical and horizontal P-waves velocity. Therefore, the P-wave velocity model resulting from wide-angle refraction experiments might be inaccurate if used for depth conversion of receiver functions, which follow near-vertical ray paths.

3.2. Intracrustal and Upper Mantle Interfaces

An intracrustal interface located at about 22 km depth is observed at 49 stations out of 70 (Table 1). This interface cannot be identified below the Vienna Basin and a few sites in the Molasse Basin. The presence of reverberated phases within the sedimentary basin and hence destructive interference may inhibit the detection of this feature. Yan and Mechie (1989) show an equivalent intracrustal interface at similar depths, and Molinari *et al*. (2012) model a layered crust, where the discontinuity between the upper and lower crust is a smooth surface located between 18 and 24 km depth. Brückl *et al*. (2007) detect a reflector at about 20 km depth, which they interpret as a thin zone of magmatic intrusion below the Bohemian massif and Molasse zone. In the southwestern area of this study, mid-crustal reflections were identified by Grad *et al*. (2009a), and below the Eastern Alps and Molasse Basin, a high velocity body in the depth interval of 18–23 km has been described (Grad *et al*. 2009a). The occurrence of high reflectivity and high velocity layers at mid-crustal depth might generate the intracrustal conversions that are observed in this study and that represent a challenge for the good application of the ZK technique. In order to gain better knowledge of the nature and depth of these interfaces, the acquisition of a larger amount of data would be necessary and would improve the sampling of crustal structures beneath each station.

An upper mantle reflector was detected in the study area by Yan and Mechie (1989) (east of the TW to the Styria Basin) and Oebberseder *et al*. (2011) (for the Vienna Basin). The interaction between European and Adriatic subcrustal lithospheres provides the basis for delamination processes, which might appear through the presence of these deep interfaces (Nicolas *et al*. 1990; Meissner and Mooney 1998). In this study, we detected the presence of an interface a few tens of km below the Moho; however, its depth is uncertain. The interface in the uppermost mantle is present below the Bohemian massif, the most elevated area of the Eeastern Alps, the southeastern part of the Vienna Basin, and the Dinarides. Since the continental lithosphere is subject to more layering than the oceanic one, the detection of the upper mantle interface could be a key insight to shed light on the genesis of the lithosphere constituting the EA.

4. Conclusions

This study presents the first results of a receiver function analysis in the Eastern Alps on a densely spaced seismic network. We apply the ZK technique to investigate the crustal thickness and additional structures in the lithosphere. The ZK method has been constrained by fixing both the V_p and V_p/V_s ratio based on previous studies. In the complex tectonic setting of the Eastern Alps, the application of the ZK technique shows the presence of multiple interfaces and results in scattered depth values of adjacent locations, ruling out the possibility of inferring larger details on Moho topography with respect to previous studies. Retrieved depths, within the uncertainty estimates, are in accordance with previous information in the area, and they give additional insights into the crustal thickness below the Vienna Basin, which was previously poorly constrained. The strong scatter of the Moho depths retrieved by RF analysis leaves room for alternative interpretations and suggests the need to perform further passive seismological studies with longer observation periods in this area.

5. Acknowledgments

We thank the teams responsible for the station deployment and data collection during the ALPASS project, led by E. Brückl, Technical University of Vienna, and G.R. Keller, University of Texas at El Paso (stations provided by IRIS/UTEP). ALPASS was funded by the Austrian Academy of Sciences. For the deployment and data collection of the CBP project, we thank G. Houseman and G. Stuart of the University of Leeds. Our thanks go to E. Kozlovskaya University of Oulu, Finland, M. Grad, University of Warsaw, and A. Guterch, Polish Academy of Sciences. Figures were created using GMT (Wessel and Smith 1998). We thank the editor and the anonymous reviewers whose suggestions helped improvethe manuscript significantly.

References

Alpine Explosion Seismology Group, Reporter H. Miller (1976), *A lithospheric seismic profile along the axis of the Alps, 1975: I: First results*, Pure Appl. Geophys. 114, 11091130.

Ammon, C. (1991), *The isolation of receiver effects from teleseismic p wave- forms*, Bull. Seismol. Soc. Am. *81*, 2504–2510.

Babuska, V., Plomerova, J., Sileny, J. (1987), Structural model of the sub- crustal lithosphere in central europe. In: Fuchs, K., Froidevaux, C. (Eds.), Composition, Structure and Dynamics of the Lithosphere-Asthenosphere System. Vol. 16. Am. Geophys. Union, Geodyn. Ser., pp. 239–251.

Behm, M. (2009), *3-d modeling of the crustal s-wave velocity structure from active source data: application to the Eastern Alps and the Bohemian Massif*, Geophysical Journal International *179*(1), 265–278.

Behm, M., Brückl, E., Chwatal, W., Thybo, H. (2007), *Application of stacking and inversion techniques to three-dimensional wide- angle reflection and refraction seismic data of the Eastern Alps*. Geophys. J. Int. 170(1), 275– 298.

Bianchi, I., Park, J., Piana Agostinetti, N., Levin, V. (2010), *Mapping seismic anisotropy using harmonic decomposition of receiver functions: an application to northern Apennines, Italy*, J. Geophys. Res. 115, b12317.

Bianchi, I., Piana Agostinetti, N., Chiarabba, C., De Gori, P. (2008), *Deep structure of the Colli Albani volcanic district (central Italy) from receiver functions analysis*, J. Geophys. Res. 113, B09313, doi:10.1029/2007JB005548.

Bischoff, M., Endrun, B., Meier, T. (2006), *Lower crustal anisotropy in central Europe deduced from dispersion analysis of Love and Rayleigh waves*, Geophys. Res. Abstr. *8* (10010).

Bleibinhaus, F., Gebrande, H. (2006), *Crustal structure of the Eastern Alps along the TRANSALP profile from wide-angle seismic tomography*, Tectonophysics *414*, 51–69.

Brückl, E. (2011), Lithospheric structure and tectonics of the Eastern Alps evidence from new seismic data. In: Closson, D. (Ed.), Tectonics. INTECH, pp. 39–64.

Brückl, E., Behm, M., Decker, K., Grad, M., Guterch, A., Keller, G. R., Thybo, H. (2010), *Crustal structure and active tectonics in the Eastern Alps*, Tectonics *29*(2).

Brückl, E., Bleibinhaus, F., Gosar, A., Grad, M., Guterch, A., Hrubcova, P., Keller, G. R., Majdaski, M., Umanovac, F., Tiira,

T., YLINIEMI, J., HEGEDS, E., THYBO, H. (2007), *Crustal structure due to collisional and escape tectonics in the eastern alps region based on profiles alp01 and alp02 from the alp 2002 seismic experiment*, Journal of Geophysical Research: Solid Earth *112*(B6).

BRÜCKL, E., BODOKY, T., HEGEDÜS, E., HRUBCOVA, P., GOSAR, A., GRAD, M., GUTERCH, A., HAJNAL, Z., KELLER, G., SPICAK, A., SUMANOVAC, F., THYBO, H., WEBER, F. (2003), *Special contribution: Alp 2002 seismic experiment*, Studia Geophysica et Geodaetica *47*(3), 671–679.

CARBONELL, R., LEVANDER, A., KIND, R. (2013), *The Mohorovičić discontinuity beneath the continental crust: An overview of seismic constraints*, Tectonophysics, *609*, 353–376, 0040-1951, http://dx.doi.org/10.1016/j.tecto.2013.08.037.

CASTELLARIN, A., NICOLICH, R., FANTONI, R., CANTELLI, L., SELLA, M., SELLI, L. (2006), *Structure of the lithosphere beneath the eastern alps (southern sector of the TRANSALP transect)*, Tectonophysics *414*(14), 259 – 282.

CHAMPION, M. E. S., WHITE, N. J., JONES, S. M., PRIESTLEY, K. F. (2006), *Crustal velocity structure of the British Isles; a comparison of receiver functions and wide-angle seismic data*, Geophys. J. Int. *166*, 795813.

DANDO, B. D. E., STUART, G. W., HOUSEMAN, G. A., HEGEDS, E., BRCKL, E., RADOVANOVI, S. (2011), *Teleseismic tomography of the mantle in the Carpathian-Pannonian region of central Europe*, Geophysical Journal International *186*(1), 11–31.

DEWEY, J. K., PITMAN, W. C., RYAN, W. B. F., BONNIN, J. (1973), *Plate tectonics and the evolution of the alpine system*, Geological Society of America Bulletin *84*, 31373180.

DI STEFANO, R., BIANCHI I., CIACCIO, M. G., CARRARA, G., KISSLING, E. (2011), *Three- dimensional Moho topography in Italy: New constraints from receiver functions and controlled source seismology*, Geochem. Geophy. Geosy. *12*.

DUGDA, M. T., NYBLADE, A. A., JULIA, J., LANGSTON, C. A., AMMON, C. J., SIMIYU, S. (2005), *Crustal structure in Ethiopia and Kenya from receiver function analysis: Implications for rift development in eastern Africa*, J. Geophys. Res. *110* (B01303), doi:10.1029/2004JB003065.

EATON, D., DINEVA, S., MEREU, R. (2006), *Crustal thickness and V_p/V_s variations in the Grenville orogen (Ontario, Canada) from analysis of teleseismic receiver functions*, Tectonophysics *420*(1–2).

ECKHARDT, C., RABBEL, W. (2011) *P-receiver functions of anisotropic continental crust: a hierarchic catalogue of crustal models and azimuthal waveform patterns*, Geophysical Journal International *187*(1), 439479.

ENDRUN, B., LEBEDEV, S., MEIER, T., TIREL, C., FRIEDERICH, W. (2011), *Complex layered deformation within the aegean crust and mantle revealed by seismic anisotropy*, Nature Geoscience *4*.

FRANÇA, G. S., ASSUMPÇAO, M. (2004), *Crustal structure of the Ribeira fold belt, SE-Brazil, derived from receiver functions*, Journal of South American Earth Sciences *16*(8), 743–758.

FREDERIKSEN, A. W., BOSTOCK, M. G. (2000), *Modeling teleseismic waves in dipping anisotropic structures*, Geophys. J. Int. 141, 401–412.

GALLACHER, R. J., BASTOW, I. D. (2012), *The development of magmatism along the Cameroon volcanic line: Evidence from teleseismic receiver functions*, Tectonics *31*(3).

GANS, C. R. (2011), Investigations of the crust and upper mantle of modern and ancient subduction zones, using Pn tomography and seismic receiver functions, PhD thesis, University of Arizona.

GEISSLER, W. H., KIND, R., YUAN, X. (2008), *Upper mantle and lithospheric heterogeneities in central and Eastern Europe as observed by teleseismic receiver functions*, Geophysical Journal International *174*(1), 351–376.

GRAD, M., BRÜCKL, E., MAJDASKI, M., BEHM, M., GUTERCH, A., CELEBRATION 2000 and ALP 2002 Working Groups (2009a), *Crustal structure of the Eastern Alps and their foreland: Seismic model beneath the Cel10/Alp04 profile and tectonic implications*, Geophysical Journal International *177*(1), 279–295.

GRAD, M., TIIRA, T., ESC Working Groups (2009b). *The Moho depth map of the European Plate*, Geophysical Journal International *176*, 279292.

GUTERCH, A., GRAD, M., KELLER, G., POSGAY, K., VOZR, J., PIK, A., BRÜCKL, E., HAJNAL, Z., THYBO, H., SELVI, O. (2003), *Special contribution: Celebration 2000 seismic experiment*, Studia Geophysica et Geodaetica *47*(3), 659–669.

KISSLING, E., SCHMID, S., LIPPITSCH, R., ANSORGE, J., FUGENSCHUH, B. (2006), Lithosphere structure and tectonic evolution of the Alpine arc: new evidence from high-resolution teleseismic tomography. In: Gee, D., Stephen- son, R. A. (Eds.), European Lithosphere Dynamics, Geol. Soc. London Mem., pp. 129–145.

KUMMEROW, J., KIND, R., ONCKEN, O., GIESE, P., RYBERG, T., WYLEGALLA, K., TRANSALP Working Group, F. S. (2004), *A natural and controlled source seismic profile through the Eastern Alps: TRANSALP*, Earth and Planetary Science Letters *225*, 115–129.

LANGSTON, C. A. (1979), *Structure under Mount Rainier, Washington, inferred from teleseismic body waves*, J. Geophys. Res. *84*(B9), 4749–4762.

LAUBSCHER, H. (1990), *The problem of the Moho in the Alps*, Tectonophysics *182*(1-2), 9–20.

LIPPITSCH, R., KISSLING, E., ANSORGE, J. (2003), *Upper mantle structure beneath the alpine orogen from high-resolution teleseismic tomography*, J. Geophys. Res *108* (2376).

LIU, H., NIU, F. (2012), *Estimating crustal seismic anisotropy with a joint analysis of radial and transverse receiver function data*, Geophysical Journal International *188*, 144164.

LLOYD, S., VAN DER LEE, S., FRANÇA, G. S., ASSUMPÇAO, M., FENG, M. (2010), *Moho map of South America from receiver functions and surface waves*, Journal of Geophysical Research *115*, b11315.

LOMBARDI, D., BRAUNMILLER, J., KISSLING, E., GIARDINI, D. (2008), *Moho depth and Poisson's ratio in the Western-Central Alps from receiver functions*, Geophys. J. Int. *173*.

LOMBARDI, D., BRAUNMILLER, J., KISSLING, E., GIARDINI, D. (2009), *Alpine mantle transition zone imaged by receiver functions*, Earth and Planetary Science Letters *278*.

LUESCHEN, E., LAMMERER, B., GEBRANDE, H., MILLAHN, K., NICOLICH, R., TRANSALP Working Group (2004), *Orogenic structure of the Eastern Alps, Europe, from TRANSALP deep seismic reflection profiling*, Tectonophysics *388*, 85102.

MEISSNER, R., MOONEY, W. (1998), *Weakness of the lower continental crust: a condition for delamination, uplift, and escape*, Tectonophysics *296*, 47–60.

MEURERS, B., REUSS, D. (2009), *A new Bouguer gravity map of Austria*, Austrian Journal of Earth Sciences *102*, 62–70.

MITTERBAUER, U., BEHM, M., BRÜCKL, E., LIPPITSCH, R., GUTERCH, A., KELLER, G. R., KOSLOVSKAYA, E., RUMPFHUBER, E. M., SUMANOVAC, F. (2011) *Shape and origin of the East-Alpine slab constrained by the alpass teleseismic model*, Tectonophysics *510*, 195–206.

Molinari, I., Raileanu, V., Morelli, A. (2012) *A crustal model for the Eastern Alps region and a new Moho map in southeastern Europe*, Pure and Applied Geophysics *169*(9), 1575–1588.

Nagaya, M., Oda, H., Akazawa, H., Ishise, M. (2008) *Receiver Functions of Seismic Waves in Layered Anisotropic Media: Application to the Estimate of Seismic Anisotropy*, Bulletin of the Seismological Society of America *98*(6), 29903006.

Nicolas, A., Hirn, A., Nicolich, R., Polino, R. (1990), *Lithospheric wedging in the western Alps inferred from the ECORS-CROP traverse*, Geology *18*(7), 587–590.

Oeberseder, T., Behm, M., Kovcs, I., Falus, G. (2011), *A seismic discontinuity in the upper mantle between the Eastern Alps and the western Carpathians: Constraints from wide-angle reflections and geological implications*, Tectonophysics *504*(1–4), 122–134.

Olsson, S., Roberts, R., Bodvarssoni, R. (2008), *Moho depth variation in the Baltic shield from analysis of converted waves*, Gff *130*.

Panza, G. F., Mueller, S., Calcagnile, G. (1980), *The gross features of the lithosphere-asthenosphere system in Europe from seismic surface waves and body waves*, Pure Appl. Geophys. *118*, 1209–1213.

Park, J. J., Levin, V. (2000), *Receiver functions from multiple-taper spectral correlation estimates*, Bull. Seismo. Soc Amer. *90*, 1507–1520.

Piana Agostinetti, N., Amato, A. (2009), *Moho depth and Vp/Vs ratio in peninsular Italy from teleseismic receiver functions*, J. Geophys. Res. *114*, B06303, doi:10.1029/2008JB005899.

Piana Agostinetti, N., Bianchi, I., Amato, A., Chiarabba, C. (2011). *Fluid migration in continental subduction: The Northern Apennines case study.* Earth and Planetary Science Letters *302*(3–4) PP. 267–278 . doi:10.1016/j.epsl.2010.10.039.

Porter, R., Zandt, G., McQuarrie, N. (2011), *Pervasive lower-crustal anisotropy in Southern California: Evidence for underplated schists and active tectonics*, Lithosphere *3*, 201–220.

Ratschbacher, L., Frisch, W., Linzer, H.-G., Merle, O. (1991), *Lateral extrusion in the Eastern Alps, part 2: Structural analysis*, Tectonics *10*(2), 257–271.

Roux, E., Moorkamp, M., Jones, A. G., Bischoff, M., Endrun, B., Lebedev, S., Meier, T. (2011), *Joint inversion of longperiod magnetotelluric dataand surfacewave dispersion curves for anisotropic structure: Application to data from central Germany*, Geophysical Research Letters *38* (L05304).

Royden, L., Horvth, F., Rumpler, J. (1983), *Evolution of the pannonian basin system: 1. Tectonics*, Tectonics *2*(1), 63–90.

Spada, M., Bianchi, I., Kissling, E., Piana Agostinetti, N., Wiemer, S. (2013), *Combining controlled-source seismology and receiver function information to derive 3d Moho topography for Italy*, Geophysical Journal International, doi:10.1093/gji/ggt148.

Tierno Ros, C. (2009), 3d density modelling of the crustal structure in the Vienna Basin region, Diploma thesis, Vienna University of Technology.

Ustaszewski, K., S. M. Schmid, B. Fügenschuh, M. Tischler, E. Kissling, and W. Spakman (2008), *A map-view restoration of the Alpine-Carpathian-Dinaridic system for the Early Miocene*, Swiss Journal of Geosciences, *101*(Supplementary Issue 1), 273–294.

Wessel, P., Smith, W. H. F. (1998,) New, improved version of the Generic Mapping Tools released, EOS Trans. AGU 79, 579.

Wittlinger, G., Farra, V., Hetényi, G., Vergne, J. and Nábělek, J. (2009), *Seismic velocities in Southern Tibet lower crust: a receiver function approach for eclogite detection*. Geophysical Journal International, *177*: 1037–1049. doi:10.1111/j.1365-246X.2008.04084.x.

Yan, Q. Z., Mechie, J. (1989), *A fine structural section through the crust and lower lithosphere along the axial region of the alps*, Geophysical Journal International *98*(3), 465–488.

Zhu, L., Kanamori, H. (2000), *Moho depth variation in southern California from teleseismic receiver function*, J. Geophys. Res. *105*, 2969–2980.

(Received June 20, 2013, revised September 23, 2014, accepted October 3, 2014, Published online October 25, 2014)